A NEW CLASS OF OPTICAL MULTISTABILITIES AND INSTABILITIES INDUCED BY ATOMIC COHERENCE

F.T. ARECCHI
Istituto Nazionale di Ottica and University, 50125 Firenze, Italy

J. KURMANN and A. POLITI
Istituto Nazionale di Ottica, 50125 Firenze, Italy

Received 26 October 1982

We investigate the collective radiative behaviour of three level atoms with two degenerate levels in the ground state, with particular emphasis on the role of the ground state atomic coherence. When put in a cavity resonator, these atoms yield not only tristability, but also a higher-order bistability, a quadristability and a region of self generated oscillations.

Recent calculations [1,2] on highly simplified models of three level atoms (doubly degenerate ground state with levels 1 and 2 radiatively coupled, via different selection rules, to a unique excited state 3), have predicted tristable behaviour when driven by two suitable fields each fulfilling one of the above mentioned selection rules. These calculations do not consider atomic coherence effects but are simply based on a population balance.

Following a more realistic scheme for Na-atoms under near resonant D_1 illumination with two circular polarization σ_+ and σ_-, we have investigated the influence of a finite coherence time on the dynamical behaviour. More precisely we have the following scheme (see also fig. 1):

i) level 1 (2) is exclusively coupled to level 3 by the $\Delta m = 1$ (-1) selection rule, thus it can only interact via σ_+ (σ_-) radiation;

ii) introducing a 3×3 density matrix ρ_{ij} $(i, j = 1, 2, 3)$ to account for occupation probabilities ρ_{ii} and atomic coherences ρ_{ij} we must take into account their decay rates, namely; the spontaneous decay rate $\gamma_1 = 0.6 \times 10^8\ s^{-1}$ of the upper population ρ_{33}; γ_2 the decay of ρ_{13} and ρ_{23} which is larger $(\gamma_2 > \gamma_1)$ and increases with the buffer gas pressure in the working cell; a much smaller $\Gamma_1 = 1.4 \times 10^3\ s^{-1}$ for the ground state population difference $\rho_{22} - \rho_{11}$ which is the source for the class of socalled pumping phenomena [3] and is

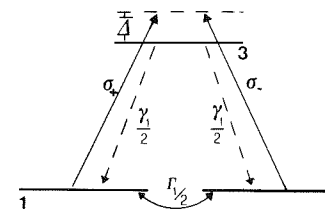

Fig. 1. Level scheme of Na-atoms under simultaneous σ_+ and σ_- irradiation at the D_1 transition; $\gamma_1/2$ spontaneous decay rate of population from level 3 to ground state; $\Gamma_1/2$ decay rate of population difference between states 1 and 2.

responsible for the very low power onset of optical bistability [4]; finally $\Gamma_2 = m\Gamma_1$ for the decay of ground state coherence $\bar{\rho}_{12}$ which is also very small and whose crucial role is already known from a large body of measurements [3,5,6]. For simplicity we do not discuss the role of Doppler broadening which can be taken into account as in ref. [4].

Experimental evidence of optical tristability has been recently given [7] by shining equal amounts of σ_+ and σ_- light on a Na filled Fabry-Perot and measuring the unbalance in the two output fields. A qualitative explanation of that effect requires only a population balance as done in ref. [1]. Here we predict some new coherence effects missed in refs. [1] and [2], that is, a finite value of Γ_2 induces qualitative differences with the previous treatments [1,2]. Indeed when shining a

0 030-4018/83/0000–0000/$ 03.00

linearly polarized field, we obtain the following new results:

i) The optical tristability region disappears for high fields and a new optical bistable branch appears. This new branch is different from the one reported in ref. [4] which was instead associated with a circularly polarized input field.

ii) For Γ_2 of the same order of magnitude as Γ_1, the evolution requires coupling of three equations and leads to oscillatory instabilities whereas the limit $m \to \infty$ of ref. [1] is described by a single equation leading only to fixed point attractors. Ref. [2], after having put $m = \infty$, reintroduces $n > 2$ equations by an unrealistic set of assumptions on the field relaxation times.

In the presence of two circularly polarized light fields, counterrotating with respective amplitudes E_+, E_- and Rabi frequencies $\alpha = \mu E_+/2\hbar$, $\beta = \mu E_-/2\hbar$, both tuned at the frequency $\omega_L = \omega_A + \bar{\Delta}$, the dynamics is rules by the following equation

$$i\dot{\rho} = [H, \rho] + \Delta\rho, \tag{1}$$

where ρ is the density 3×3 matrix, the dot stays for the time derivative, D stays for the above described damping mechanisms and the hamiltonian matrix H in the interaction representation is given by

$$H = -\begin{pmatrix} 0 & 0 & \alpha \\ 0 & 0 & \beta \\ \alpha^* & \beta^* & \bar{\Delta} \end{pmatrix} \tag{2}$$

As in ref. [4] we consider e.m. intensity levels low enough to never reach saturation on the 1–3, 2–3 transitions, that is,

$$\alpha\alpha^*/\gamma_1\gamma_2 \ll 1, \qquad \beta\beta^*/\gamma_1\gamma_2 \ll 1. \tag{3}$$

As a consequence, for any situation, level 3 is practically empty ($\rho_{33} = 0$) and the off-diagonal elements ρ_{13} and ρ_{23} relax so rapidly that $\dot{\rho}_{13} = \dot{\rho}_{23} = 0$ and we can take for them the equilibrium values (adiabatic elimination).

Hence the dynamics is like that of a two level system ($i, j = 1, 2$). Introducing the quantities

$$R_1 = \rho_{12} + \rho_{21}, \quad R_2 = i(\rho_{21} - \rho_{12}), \quad R_3 = \rho_{22} - \rho_{11} \tag{4}$$

with the normalization $\rho_{22} + \rho_{11} = 1$

and

$$S_1 = \frac{\alpha^*\beta + \beta^*\alpha}{\Gamma_1\gamma_2}, \qquad S_2 = \frac{i(\alpha^*\beta - \beta^*\alpha)}{\Gamma_1\gamma_2},$$

$$S_3 = \frac{\beta\beta^* - \alpha\alpha^*}{\Gamma_1\gamma_2}, \qquad S_0 = \frac{\beta\beta^* + \alpha\alpha^*}{\Gamma_1\gamma_2}, \tag{5}$$

the relevant atomic equations become

$$\dot{R}_1/\Gamma_1 = G_2(S_2R_3 - S_3R_2) - G_1S_1 - (G_1S_0 + m)R_1,$$

$$\dot{R}_2/\Gamma_1 = G_2(S_3R_1 - S_1R_3) - G_1S_2 - (G_1S_0 + m)R_2,$$

$$\dot{R}_3/\Gamma_1 = G_2(S_1R_2 - S_2R_1) - G_1S_3 - (G_1S_0 + 1)R_3. \tag{6}$$

Here we have introduced

$$G \equiv G_1 - iG_2 = (1 - i\Delta)/(1 + \Delta^2), \tag{7}$$

where $\Delta = \bar{\Delta}/\gamma_2$ is the field-atoms detuning normalized to the transverse decay rate γ_2.

The first terms in the right hand sides of eqs. (6) represent a typical hamiltonian spin–spin interaction between the atoms (R) and the field (S) pairs. The last terms are the decays induced by collision processes. The other terms represent the damping and pumping terms coming from the depletion of population of level 3

Notice that in the atomic equations the two fields do not appear separately but via the combinations (5). Hence the process here considered belongs to the class of two photon processes as other effects previously considered [8].

Let us now write the coupled Maxwell equations for the two fields α, β in the limit of slowly varying envelope approximation and of the mean field theory [9]

$$\dot{\alpha} = -\frac{i\omega}{4\epsilon_0}\frac{\mu^2 N}{\sqrt{2}\hbar}\rho_{13} + k[i\theta_\alpha - \alpha + \alpha_S],$$

$$\dot{\beta} = -\frac{i\omega}{4\epsilon_0}\frac{\mu^2 N}{\sqrt{2}\hbar}\rho_{23} + k[i\theta_\beta - \beta + \beta_S], \tag{8}$$

where $\sqrt{T}\alpha_S = \alpha_0$, $\sqrt{T}\beta_S = \beta_0$ are the input fields expressed in Rabi frequency units, $1/k$ is the field decay time in the cavity, T is the mirror transparency and θ is the mistuning between the optical frequency ω_L and the cavity eigenfrequency ω_C in units of the cavity damping rate k, that is $\theta = (\omega_L - \omega_C)/k$.

By replacing the equilibrium solutions for ρ_{13} and ρ_{23}

$$\rho_{13} = -(iG/2\gamma_2)[\alpha(1 - R_3) + \beta(R_1 + iR_2)],$$

$$\rho_{23} = -(iG/2\gamma_2)\,[\beta(1+R_3)+\alpha(R_1-iR_2)], \qquad (9)$$

into eqs. (8) we finally obtain

$$\dot{\alpha} = k\{-CG[\alpha(1-R_3)+\beta(R_1+iR_2)]+i\theta_\alpha-\alpha+\alpha_S\},$$

$$\dot{\beta} = k\{-CG[\beta(1+R_3)+\alpha(R_1-iR_2)]+i\theta_\beta-\beta+\beta_S\},$$

where (10)

$$C = \omega\mu^2 N/8\sqrt{2}\gamma_2 k\epsilon_0\hbar \qquad (11)$$

is the usual cooperation number [9].

By solving at equilibrium the system of eqs. (6) and (10) we obtain the following relations among the input intensities

$$Y_+ = \alpha_S\alpha_S^*/\Gamma_1\gamma_2, \qquad Y_- = \beta_S\beta_S^*/\Gamma_1\gamma_2 \qquad (12)$$

and output intensities

$$X_+ = \alpha\alpha^*/\Gamma_1\gamma_2, \qquad X_- = \beta\beta^*/\Gamma_1\gamma_2, \qquad (13)$$

$$\frac{Y_\pm}{X_\pm} = \left\{\frac{C[m(S_0^2+(1+m)S_0+mD)\mp(1-m)S_3S_0\mp(1-m)mS_0]}{F(S_0,S_3)}+1\right\}^2 + \left\{\frac{\Delta C[m(S_0^2+(1+m)S_0+mD)+(1-m)S_3^2\mp(1-m)mS_3]}{F(S_0,S_3)}+\theta\right\}^2, \qquad (14)$$

where $D = 1+\Delta^2$ and

$$F(S_0,S_3) = [S_0^2+(1+m)S_0+mD] \times (S_0+mD)+\Delta^2(1-m)S_3^2 \qquad (15)$$

is a common denominator.

Since $k = 10^8\ s^{-1}$ we adiabatically eliminate the field equations (10) and reduce the system from seven to three coupled equations whose stability analysis around the stationary solution (14) can be performed as usual by a linearization procedure.

All successive calculations refer for simplicity to a symmetric input intensity $Y = Y_+ = Y_-$.

In fig. 2 we have chosen a coherence ratio $m = 20$, $C = 80$, $\theta = 0.5$ and we plot the output X versus Y for two different Δ values, namely 1.5 and 2. In both cases, the main branch, having a large S shape, corresponds to symmetric output $X_+ = X_-$ ($S_3 = 0$ in the notation (5)). The second closed loop, which bifurcates from the S branch at points 3 and 5, corresponds to different X_+ and X_- ($S_3 \neq 0$) and if the lower branch

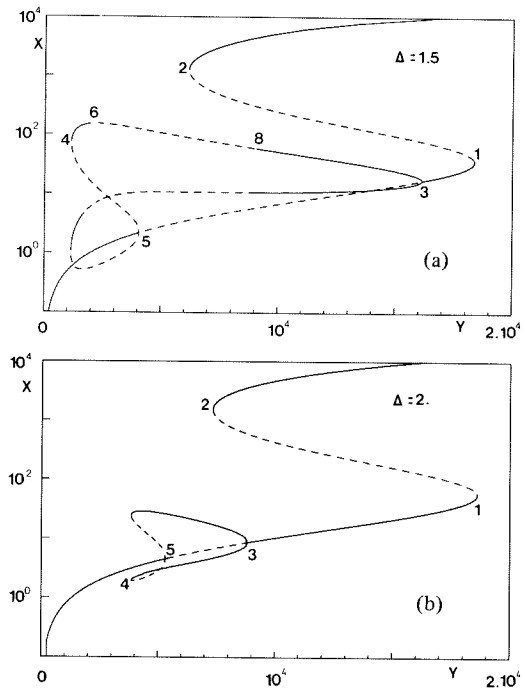

Fig. 2. One of the output intensities (X_+, X_-) versus the linearly polarized input intensity $Y = Y_+ = Y_-$ for $C = 80$, $\theta = 0.5$, $m = 21$ and different Δ: a) $\Delta = 1.5$, b) $\Delta = 2$. The numbers show the turning and bifurcation points. In a), between 2 and 5, the system displays oscillatory behaviour; in b) the system shows only fixed point type solutions. The intensities are normalized as in eqs. (12), (13).

is read as X_+ the upper one must be attributed to X_- and vice versa. In the limit $m \to \infty$ the bifurcation point 3 and the turning points 1 and 2 of the $S_3 = 0$ branch go to infinity. Therefore the associated bistability, which in our plots appears above the tristability region, is no longer present. Such a bistability appearing with linear, rather than circular [4] polarization is therefore an atomic coherence feature. This appears also from the fact that Y values of turning points 1 and 2 increase linearly with m (this is shown in detail in fig. 4).

In fig. 2a there are two tristable regions, one between the turning point 4 and bifurcation point 6, the other between bifurcation points 8 and 3. The other regions of the inner loop correspond to unstable cases. In the range between 5 and 2 we have verified oscillatory behaviour (see fig. 6); between 6–5 and 2–8, the presence of a stable branch may coexist with oscillatory behaviour. For $\Delta = 2$ (fig. 2b) points 6 and 8 merge and the whole inner loop, from 4 to 3, becomes stable. Intervals 4–5 and 2–3 are associated with stable regions

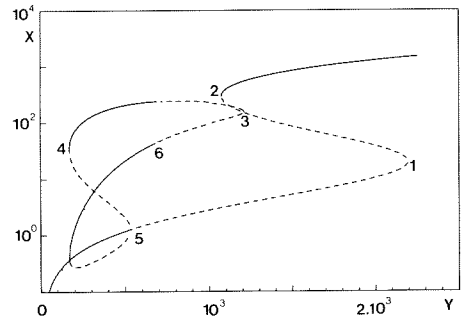

Fig. 3. One of the output intensities (X) versus the input intensity (Y). Bifurcation point 3 lies on the negative slope branch of the S shape curve. The parameters are $C = 30$, $\Delta = 1.0$, $\theta = -0.5$ and $m = 18$.

of the S loop, thus yielding tristability, while between 5 and 2 this S loop provides an unstable branch. Notice that in the tristable region of fig. 2a, both X_+ and X_- jump above the common value of the $S_3 = 0$ branch. In fig. 2b however, between 4 and 5, X_+ and X_- have increments of different sign. This corresponds to the experimental situation of ref. [8].

To show how rich is the phenomenology for realistic ranges of the control parameters, we display in fig. 3 an example where the bifurcation point 3 stems from the negative slope section of S branch, while in fig. 2 it was stemming from the lower section of the S branch. Comparing with fig. 2 we notice that no extra relevant point exists between points 5 and 1, hence all this section of the lower branch is unstable.

The details of the dynamical behaviour can be appreciated in the phase diagram of fig. 4, which shows the contour lines corresponding to the relevant points 1 to 8 of the equilibrium characteristics (either turning points or bifurcation points) versus two of the control parameters, namely the input intensity Y and the coherence ratio m, for fixed $C = 30$, $\Delta = 1.0$ and $\theta = -0.5$. Domains characterized by different dynamical behaviour have been denoted in fig. 4 by different hatchings. Precisely, white regions (no hatching) denote monostable regions and the five different hatchings correspond to the following regions: a) tristability: b) bistability; c) limit cycle oscillations; d) coexistence of monostability and limit cycle oscillations; e) quadristability.

For the chosen set of fixed parameters C, Δ, and θ, region e is rather small and it can be visualized only in the magnified version of the phase diagram given in fig. 4b.

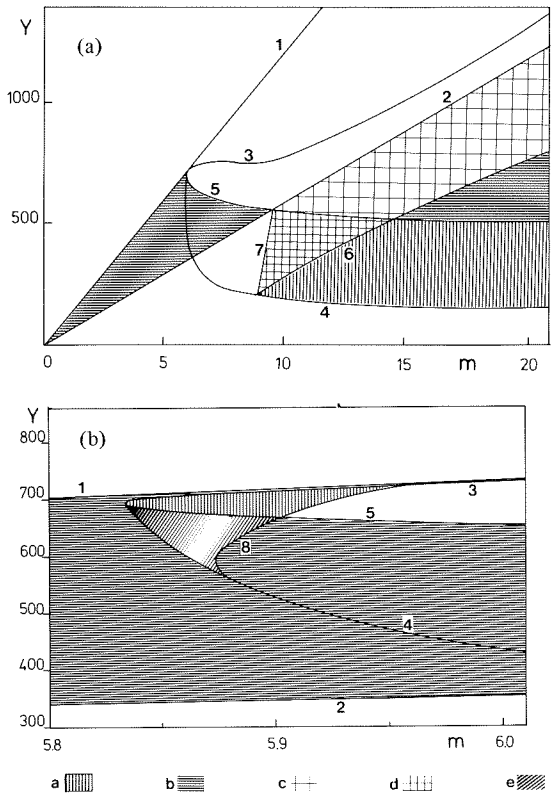

Fig. 4. Phase diagram versus the input intensity Y and the coherence ratio m for fixed $C = 30$, $\theta = -0.5$ and $\Delta = 1.0$. The numbered lines show the dependence of the characteristic points and bound the different phase domains. Hatching (a) corresponds to tristability, (b) to bistability, (c) to an oscillatory domain, (d) to coexistence of monostability and oscillations, (e) to quadristability (see the enlarged part of the phase diagram in fig. 4b).

Choosing $m = 11$ and varying the input intensity within the unstable regions c, d of fig. 4 we have numerically studied the changes in the period and amplitude of the output oscillations. For $Y = 384$, slightly above the Hopf bifurcation point 6, the amplitude of the limit cycle is very small and the period ($\sim 2/(5\Gamma_1)$) can be easily extrapolated from the imaginary part of the eigenvalues of the linear stability analysis. Increasing Y both the period and the amplitude increase giving rise to well separated high spikes. Finally, close to the upper boundary of the unstable region the oscillation disappears in accordance to an unusual type of bifurcation. The period diverges to infinity, but there is a large growth of residence times on the low intensity level and on a new intermediate value (~ 200). Such a behav-

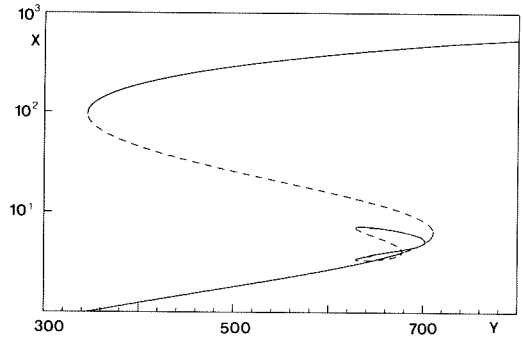

Fig. 5. The output intensity (X) versus the input intensity (Y) in the quadristability region with $C = 30$, $\theta = -0.5$, $\Delta = 1.0$, $m = 5.85$.

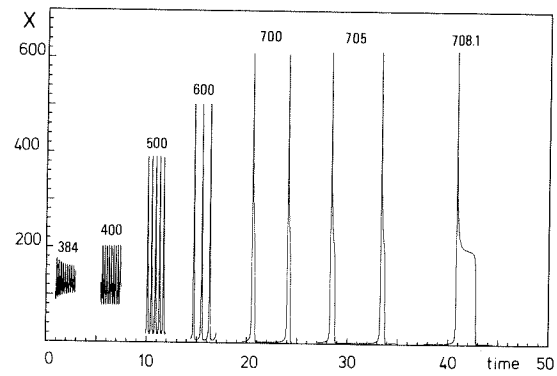

Fig. 6. Samples of oscillations for $C = 30$, $\theta = -0.5$, $\Delta = 1.0$ and $m = 12$ corresponding to different Y (384, 400, 500, 600, 700, 705, 708.1). The first one is slightly above the the Hopf bifurcation point 6 (see fig. 4). It has been drawn a single peak of the last limit cycle whose period is about 20. The time is normalized to D/Γ_1.

iour describes the collapse onto two stationary linearly polarized solutions, an unstable one on the lower branch, and a stable one on the upper branch close to the turning point 2.

Our dynamics being ruled by three equations, we should expect not only limit cycle oscillations but also chaotic behaviour. In the limited region explored thus far we have been able to show evidence of limit cycle behaviour.

To summarize, with respect to previous schemes of tristability [1,2] our consideration of realistic alkali atoms has given the following new features:

i) A bistability branch which is neither the two level bistability [10] with the saturation parameter as in eq. (3) nor the bistability by optical pumping associated with normalization (13). In such a case the dependence on the coherence effect is emphasized by the associated saturation parameter which is $\alpha\alpha^*/\Gamma_2\gamma_2$.

ii) The appearance of a quadristability region (see fig. 5) interlaced with tristable behaviour.

iii) The appearance of limit cycle oscillations, which are incompatible with the simplified dynamics of ref. [1]. The dynamics of ref. [2] leads also to periodic oscillations as well as to chaos. There, however, the conservation of time dependent field equations implies damping times for the field much longer than the atomic ones, which has been here shown to be incompatible with the optical pumping phenomenon, based on a very slow transfer of population and coherence between the two ground state levels.

This work was supported in part by the Italian National Research Council (Contract Consiglio Nazionale delle Ricerche - Istituto Nazionale di Otica). One of us (J.K.) was the recipient of a fellowship from the "Fonds zur Foerderung der Weiterbildung junger Wissenschafter" of the University of Basel.

References

[1] M. Kitano. T. Yabuzaki and T. Ogawa, Phys. Rev. Lett. 46 (1981) 927.
[2] C.M. Savage, H.J. Carmichael and D.F. Walls, Optics Comm. 42 (1982) 211;
H.J. Carmichael, C.M. Savage and D.F. Walls, to be published.
[3] F. Strumia, Suppl. al Nuovo Cimento 26 (1968) 355.
[4] F.T. Arecchi, G. Giusfredi, E. Petriella and P. Salieri, Appl. Phys. B to appear.
[5] G. Orriols, Nuovo Cimento 52 (1979) 1.
[6] G. Alzetta, L. Moi and G. Orriols, Nuovo Cimento 52B (1979) 209.
[7] S. Cecchi, G. Giusfredi, E. Petriella and P. Salieri, submitted to Phys. Rev. Lett.
[8] D. Grischkowsky, M.M. T. Loy and P.F. Liao, Phys. Rev. 12A (1975) 2514;
F.T. Arecchi and A. Politi, Lett. Nuovo Cim. 23 (1978) 65;
G.P. Agrawal and C. Flytzanis, Phys. Rev. Lett. 44 (1980) 1059.
[9] R. Bonifacio and L.A. Lugiato, Phys. Rev. 18A (1978) 1129.
[10] R. Bonifacio and L.A. Lugiato, Optics Comm. 19 (1976) 172.